JOURNAL OF GEOPHYSICAL RESEARCH, VOL. 107, NO. B12, 2372, doi:10.1029/2001JB000893, 2002

Steady subsidence of Medicine Lake volcano, northern California, revealed by repeated leveling surveys

Daniel Dzurisin
U.S. Geological Survey, David A. Johnston Cascades Volcano Observatory (USGS/CVO), Vancouver, Washington, USA

Michael P. Poland[1]
Department of Geology, Arizona State University, Tempe, Arizona, USA

Roland Bürgmann
Department of Earth and Planetary Science, University of California, Berkeley, Berkeley, California, USA

Received 3 August 2001; revised 13 May 2002; accepted 11 September 2002; published 27 December 2002.

[1] Leveling surveys of a 193-km circuit across Medicine Lake volcano (MLV) in 1954 and 1989 show that the summit area subsided by as much as 302 ± 30 mm (−8.6 ± 0.9 mm/yr) with respect to a datum point near Bartle, California, 40 km to the southwest. This result corrects an error in the earlier analysis of the same data by *Dzurisin et al.* [1991], who reported the subsidence rate as −11.1 ± 1.2 mm/yr. The subsidence pattern extends across the entire volcano, with a surface area of nearly 2000 km^2. Two areas of localized subsidence by as much as 20 cm can be attributed to shallow normal faulting near the volcano's periphery. Surveys of an east–west traverse across Lava Beds National Monument on the north flank of the volcano in 1990 and of a 23-km traverse across the summit area in 1999 show that subsidence continued at essentially the same rate during 1989–1999 as 1954–1989. Volcano-wide subsidence can be explained by either a point source of volume loss (Mogi) or a contracting horizontal rectangular dislocation (sill) at a depth of 10–11 km. Volume loss rate estimates range from 0.0013 to 0.0032 km^3/yr, depending mostly on the source depth estimate and source type. Based on first-order quantitative considerations, we can rule out that the observed subsidence is due to volume loss from magma withdrawal, thermal contraction, or crystallizing magma at depth. Instead, we attribute the subsidence and faulting to: (1) gravitational loading of thermally weakened crust by the mass of the volcano and associated intrusive rocks, and (2) thinning of locally weakened crust by Basin and Range deformation. The measured subsidence rate exceeds long-term estimates from drill hole data, suggesting that over long timescales, steady subsidence and episodic uplift caused by magmatic intrusions counteract each other to produce the lower net subsidence rate. *INDEX TERMS:* 8499 Volcanology: General or miscellaneous; 1206 Geodesy and Gravity: Crustal movements—interplate (8155); 1299 Geodesy and Gravity: General or miscellaneous; 8419 Volcanology: Eruption monitoring (7280); 8439 Volcanology: Physics and chemistry of magma bodies; *KEYWORDS:* Medicine Lake volcano; crustal subsidence; leveling surveys; gravitational loading; ground deformation; Cascade Range

Citation: Dzurisin, D., M. P. Poland, and R. Bürgmann, Steady subsidence of Medicine Lake volcano, northern California, revealed by repeated leveling surveys, *J. Geophys. Res.*, *107*(B12), 2372, doi:10.1029/2001JB000893, 2002.

1. Geologic Setting and Eruptive History

[2] Medicine Lake volcano (MLV) is located about 50 km ENE of Mount Shasta between the towns of Tulelake, Bartle, and Tennant in northern California (Figures 1 and 2). MLV lavas cover nearly 2000 km^2 and their volume is about 600 km^3, making MLV the largest volcano by volume in the Cascade Range [*Donnelly-Nolan*, 1988]. The broad MLV shield with its 7 × 12 km, 0.3-km-deep summit caldera (where the body of water called Medicine Lake is located) comprises mainly basalt and andesite lavas, but several late Holocene eruptions produced dominantly rhyolite lavas. During the most recent eruptive episode between 3000 and 900 radiocarbon years ago, eight eruptions produced about 2.5 km^3 of lavas that are predominantly rhyolite but range in composition through dacite and andesite to basalt [*Donnelly-Nolan et al.*, 1990].

[3] Eruptive activity at MLV is driven by basaltic intrusions that are facilitated by crustal extension in the western

[1]Now at USGS/CVO, Vancouver, Washington, USA.

0148-0227/02/2001JB000893$09.00

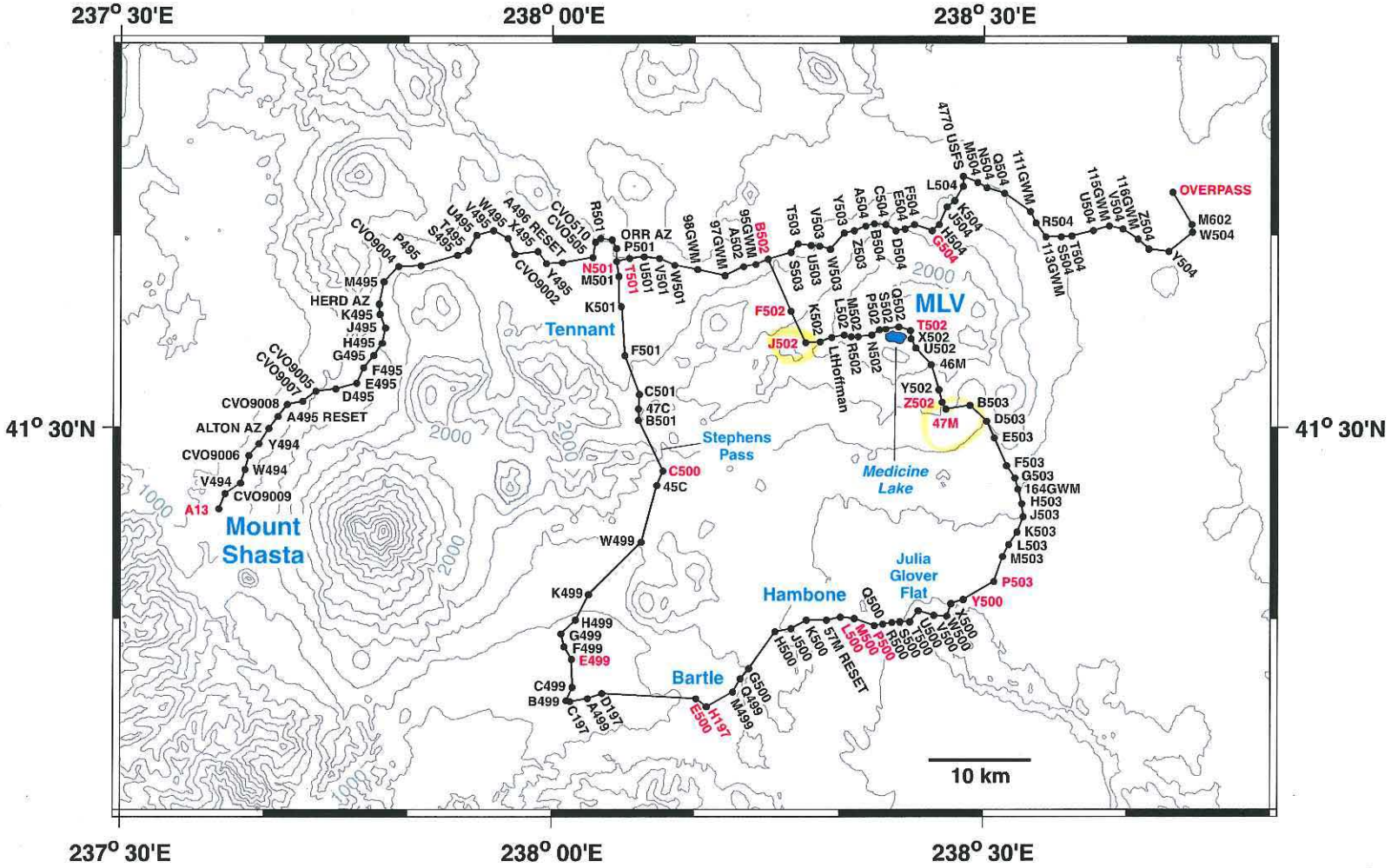

Figure 1. Leveling traverses (dark lines) near Medicine Lake volcano. Dots along the traverses represent benchmarks with corresponding labels. The circuit across the volcano (Bartle–Hambone–MLV–Tennant–Bartle) was measured in 1954 and 1989; the segment across the summit caldera between benchmarks 47 M and J502 was measured in 1988 and 1999. The west–east traverse from A13 near Mount Shasta to OVERPASS was measured entirely in 1954 and partly in 1990 (Figure 3). Datum point H197 is located near Bartle. Benchmarks mentioned in the text, shown in red here, are also shown in Figure 3. Contour interval for the generalized topography is 200 m.

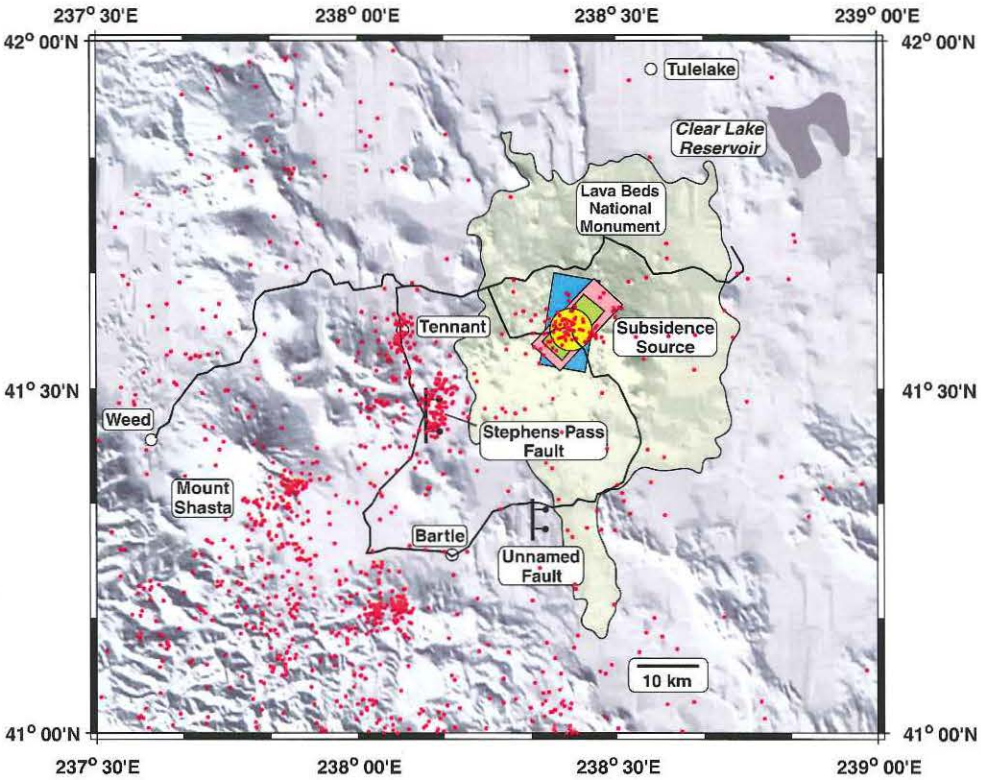

Figure 2. Leveling routes (thick lines) near Medicine Lake volcano (yellow shading) and best fit deformation sources discussed in the text. The Stephens Pass fault and an unnamed fault (bars on downthrown sides) are modeled from the 1954–1989 displacements of nearby benchmarks as normal-slip dislocations on east-dipping faults (Table 2). The Mogi source (yellow circle) is located beneath the south part of Medicine Lake caldera. The model sills (rectangles) are based on displacements measured from 1954 to 1989 (pink), 1989 to 1999 (blue), and all data combined (green). Red dots represent earthquake epicenters for the period 1909–1999 from the University of California Berkeley Seismographic Stations catalog. A sparse seismic network could not locate earthquakes smaller than $M \sim 4.5$ from 1909 to the 1950s or smaller than $M \sim 3$ from the 1950s to 1980. With those limitations, the network located no earthquakes near MLV prior to 1975. Notable clusters of earthquakes include the 1978 Stephens Pass swarm, 1981 Tennant swarm, and 1988–1989 Medicine Lake swarm, the latter located beneath the summit caldera near the yellow circle. Few earthquakes have been located near the modeled unnamed fault, although vertical displacements of several cm were measured at three nearby benchmarks (L500, M500, P500) between 1954 and 1989. The Tennant swarm produced no measurable surface displacements and therefore we did not model its source.

Basin and Range tectonic province. Vents are typically aligned within 30° of N, parallel or subparallel to major faults that trend dominantly NNW to N [*Donnelly-Nolan et al.*, 1990]. This pattern is generally consistent with the orientation of maximum principal stress in the region [*Zoback and Zoback*, 1989; *Zoback*, 1992]. Evidence for a large intrusive complex beneath MLV includes: 1) a positive Bouguer gravity anomaly in the upper few km of the crust [*Finn and Williams*, 1982]; 2) a corresponding zone of anomalously high compressional wave velocity inferred from active seismic tomography [*Evans and Zucca*, 1998]; and 3) a much larger zone of high compressional wave velocity extending into the upper mantle, which is inferred from teleseismic tomography [*Ritter and Evans*, 1997]. The active tomography study also revealed a low-velocity, high attenuation (low-Q) region 2–6 km beneath the caldera that *Evans and Zucca* [1998] interpreted as a small silicic magma reservoir.

2. Regional Deformation and Seismicity

[4] There is abundant geodetic evidence for contemporary crustal extension in the Basin and Range, although the details are poorly understood in the vicinity of MLV. *Thatcher et al.* [1999] measured a dense GPS traverse across the province at latitudes between 38°N and 40°N (MLV is located at ~41.6°N), and showed that: 1) the Sierra Nevada block is moving 12.5 ± 1.5 mm/yr N52°W relative to stable North America, and 2) deformation is

strongly concentrated in the westernmost ~200 km and easternmost ~100 km of the 800 km traverse. This result generally agrees with earlier measurements of integrated Basin and Range extension by *Dixon et al.* [1995] (12.1 ± 1.2 mm/yr N38°W ± 5°), *Argus and Gordon* [1991] (11 ± 1 mm/yr N28°W ± 3°), *Bennett et al.* [1998] (11 ± 2 mm/yr NW), and *Minster and Jordan* [1987] (9.2 ± 2.6 mm/yr N64°W ± 9°). Deformation in the western Basin and Range includes a dominant, right-lateral component associated with the eastern California shear zone–Walker Lane belt. The continuation and distribution of eastern California shear zone deformation north of 41°N and its interaction with Cascadian back arc tectonics are not well understood [*Blakely et al.*, 1997; *Dixon et al.*, 2000; *Miller et al.*, 2001].

[5] Numerous young normal faults and sporadic seismicity in the MLV region suggest present-day Basin and Range deformation [*Blakely et al.*, 1997]. Seismic records collected by the University of California Berkeley Seismographic Stations starting in 1909 show no earthquakes in the MLV region prior to 1950, but sparse instrumental coverage during that period means that events smaller than *M*4 probably would not have been located [*Bolt and Miller*, 1975]. Since stations were added in the 1950s and 1980, earthquakes have been located throughout the region but mostly west of MLV (Figure 2).

[6] Three notable earthquake swarms have been recorded near MLV. The first, in August 1978, was centered about 15 km south of Tennant and 5 km south of Stephens Pass, approximately midway between MLV and Mount Shasta (hereafter called the 1978 Stephens Pass swarm). The largest event in the sequence (*M*4.6 on 1 August) was followed by hundreds of aftershocks during the next two weeks. The activity produced a north trending, 2-km-long, 75-m-wide zone of tensional fractures, grabens, and collapse depressions, including open fissures that cut Stephens Pass Road 5 km south of Stephens Pass. Benchmark C500 is located within the ground breakage zone (Figures 1 and 2) and apparently moved downward ~20 cm as a result of the swarm (see section 3.3). The 8-km-long aftershock zone dips eastward from the surface breaks to ~4 km depth. Focal mechanisms suggest E–W extension on a N-striking fault, consistent with the regional fault pattern [*Cramer*, 1978; *Bennett et al.*, 1979].

[7] Another swarm of shallow earthquakes occurred during January–February 1981 almost directly beneath Tennant (hereafter called the 1981 Tennant swarm). The largest event (*M*4.1) on 9 January was followed by 11 $M \geq 3.0$ events within the next 24 hours. Activity declined sporadically during the next several weeks. No surface breaks were reported and no offsets are apparent in the 1954–1989 or 1954–1990 displacement profiles where they cross the epicentral zone (see sections 3.3 and 3.4 and Figures 1–5).

[8] The only earthquake swarm located at MLV itself occurred in 1988–1989 beneath the summit caldera. More than 80 events per hour were recorded during the swarm's peak on 29 September 1988, including the largest of the sequence (*M*4.1). Sporadic flurries of smaller events ($M \leq 3.1$) occurred throughout the rest of 1988 and 1989. The 1988–1989 earthquakes were all shallow, mostly within 2 km of the surface [*Walter and Dzurisin*, 1989]. *Dzurisin et al.* [1991] attributed the swarm to subsidence-induced bending and episodic fracturing of cold, brittle rocks mostly within the MLV edifice.

3. Leveling Results

3.1. Error Estimates

[9] All of the MLV leveling surveys described here were conducted in accordance with established procedures for second order surveys (1954) or first-order, class II surveys (1988, 1989, 1990, 1999), and all appropriate corrections were applied to the data [*Dzurisin et al.*, 1991; *Balazs and Young*, 1982; *Federal Geodetic Control Committee*, 1984; *Schomaker and Berry*, 1981; *Stein*, 1981; *Strange*, 1980a, 1980b; *Vanicek et al.*, 1980]. Throughout this paper, error estimates include both a length-dependent term to account for random surveying error [*Vanicek et al.*, 1980] and a time-dependent term to account for vertical benchmark instability [*Wyatt*, 1989]. In the first case, the standard deviation of a vertical displacement measured by comparison of two leveling surveys is given by

$$\sigma(L) = \left(\beta_1^2 + \beta_2^2\right)^{1/2} \cdot L^{1/2}$$

where β_1 and β_1, in units of mm/km$^{1/2}$, are constants for each order, class, and vintage of leveling and L is the distance in kilometers along the traverse. The appropriate values of β are 0.7 mm/km$^{1/2}$ for contemporary first-order, class II surveys (including the 1988, 1989, 1990, and 1999 surveys described here) and 3 mm/km$^{1/2}$ for second-order, class II surveys conducted during 1917–1955 (including the 1954 survey described here) [*Vanicek et al.*, 1980]. Thus, the 1-sigma uncertainty in displacements from random surveying error is 3.1 mm/km$^{1/2}$ · L (km)$^{1/2}$ for comparisons involving the 1954 survey and any subsequent survey, and 1.0 mm/km$^{1/2}$ · L (km)$^{1/2}$ for comparisons involving any two subsequent surveys.

[10] Benchmark instability, which accumulates with time rather than distance, is another source of uncertainty in leveling results. *Wyatt* [1989] analyzed cumulative long-period vertical motions of benchmarks at Piñon Flat Observatory, California, and showed that including an error term dependent on the square root of time (or a slightly higher power) improves estimates of true ground deformation. Accordingly, we included the following term in our error estimates throughout this paper

$$\sigma(t) = \alpha \cdot t^{1/2}$$

where α = 0.5 mm/yr$^{1/2}$. For the 35-year interval between the 1954 and 1989 surveys, for example, this term contributes ±3.0 mm to the uncertainty in displacements and 0.1 mm/yr to the uncertainty in displacement rates. For the 10-year interval from 1989 to 1999, the corresponding values are ±1.6 mm and 0.2 mm/yr. For modeling purposes, inclusion of a non-length-dependent term is important so closely spaced benchmarks do not receive undue weight.

[11] In summary, the net uncertainty in vertical displacements is given by

$$\sigma(L,t) = \sigma(L) + \sigma(t)$$

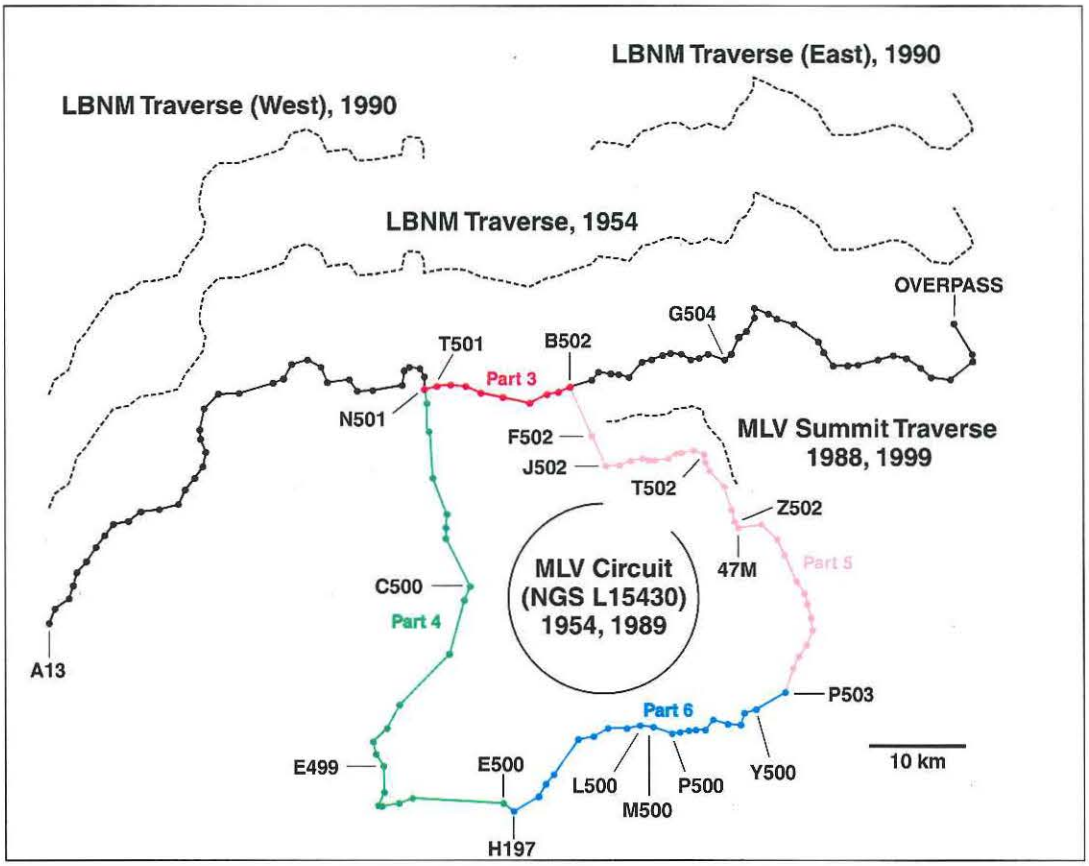

Figure 3. Leveling routes near Medicine Lake volcano and survey dates. The 1954 survey was conducted by the National Geodetic Survey using second-order, class II procedures. The 1988, 1989, 1990, and 1999 surveys were conducted by the USGS Volcano Hazards Program using first-order, class II procedures. Benchmarks mentioned in the text are labeled. The MLV circuit comprises NGS line L15430, parts 3 (red), 4 (green), 5 (pink), and 6 (blue).

and the uncertainty in annual displacement rates is given by

$$\sigma(L,t,N) = \frac{\sigma(L,t)}{N}$$

where N is the number of years between surveys.

3.2. Earlier Results

[12] An extensive leveling survey near MLV was conducted in 1954 by the National Geodetic Survey (NGS) using second-order, class II procedures. It included a 193 km circuit across the summit area of MLV by way of Bartle, Medicine Lake, Stephens Pass, and Tennant, plus a 148 km traverse between Weed and California Highway 139 through Lava Beds National Monument (LBNM, Figures 1–3). An 18.5 km segment between T501 and B502 (~5 km NNE of Tennant and midway between Tennant and Medicine Lake, respectively) was common to both surveys.

[13] The U.S. Geological Survey's Volcano Hazards Program (USGS VHP) remeasured the MLV circuit in 1989 and the LBNM traverse in 1990 using first-order, class II procedures. These surveys were prompted by results of smaller surveys across the summit caldera in August 1988 and October 1988, a period that included the peak of the 1988–1989 Medicine Lake earthquake swarm. Comparisons showed that T502, which is near the center of the caldera along the NE shore of Medicine Lake, subsided -167.2 ± 10.8 mm from 1954 to August 1988 (-4.9 ± 0.3 mm/yr) and -8.3 ± 3.5 mm from August 1988 to October 1988, both with respect to J502 (~10 km west of Medicine Lake, Figure 1) [*Dzurisin et al.*, 1991]. In both cases, the subsidence pattern extended beyond the ends of the summit traverse (J502 and 47M, the latter ~10 km SSE of Medicine Lake), so the entire MLV circuit was remeasured in 1989 for comparison to the 1954 survey. The resulting discovery of volcano-wide subsidence led the VHP to remeasure the LBNM traverse in 1990 and the summit traverse in 1999 (Figure 3).

[14] *Dzurisin et al.* [1991] compared results of the 1954, 1988, and 1989 surveys and concluded that the summit area of MLV subsided at an average rate of -11.1 ± 1.2 mm/yr during 1954–1989. We have discovered an error in that analysis that we correct in this paper. The volcano-wide pattern of subsidence centered in the summit caldera is mostly unchanged, but some offsets in the 1954–1989 displacement profile that were attributed to faulting are now recognized as mistakes in the earlier analysis. In

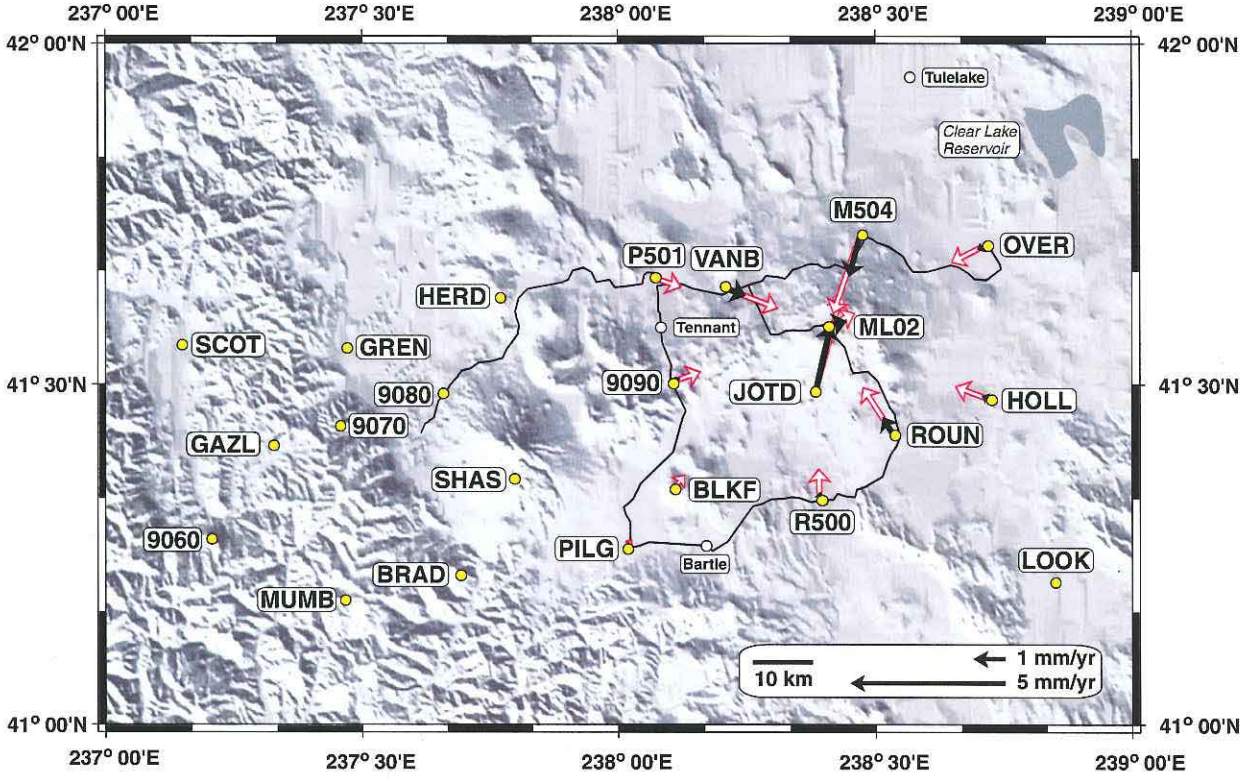

Figure 9. Predicted horizontal displacement rates at existing GPS stations based on the best fitting Mogi source (red arrows) and sill (black arrows).

1999 only), which raises the question of how far into the past the current rate should be extrapolated. For example, a constant subsidence rate of 8.6 ± 0.8 mm/yr would produce 8.6 ± 0.8 m of subsidence in 1,000 years and 860 ± 80 m of subsidence in 100,000 years. *Dzurisin et al.* [1991] reviewed the evidence for long-term subsidence of MLV from 8 drill holes, 5 of which penetrated the entire volcanic pile. They concluded that the crust beneath MLV has been downwarped ~500 m relative to the surrounding plateau. The current rate would have produced 500 m of subsidence in only ~60,000 years, approximately 10% of the lifespan of the volcano. It is highly unlikely that all of the subsidence would occur in the last 10% of the volcano's history, especially given that there is no obvious increase in eruptive productivity. Thus, the current rate of subsidence must be anomalous and either the subsidence rate has increased through time, the subsidence process has been episodic, or subsidence has been counterbalanced by uplift associated with intrusions.

[36] The relatively high rate of contemporary subsidence could be a recent phenomenon, i.e., a delayed response of the lithosphere to the increasing load imposed by the growing MLV edifice plus intrusive complex. For example, changes in the subsurface temperature distribution caused by intrusions or eruptions could lead to time-varying viscous strength of the crust. Extension could be responsible for a relatively minor amount of subsidence throughout the entire 500–600 ka lifespan of MLV, while gravitational loading by the mature volcanic system has only recently become the dominant mechanism and is largely responsible for the high contemporary subsidence rate. Alternatively, crustal extension might be the dominant cause of subsidence and the extension rate might have increased recently. In this scenario, gravitational loading produced a relatively minor, steady amount of subsidence as the volcano grew, while the crustal extension rate increased to produce the relatively high contemporary subsidence rate. Thus, the current anomalous subsidence rate could be explained by an unusually high crustal extension rate in the MLV region during Holocene time. This possibility is neither supported nor refuted by available data. Regardless of the subsidence mechanism, the historical rate of subsidence is clearly greater than the average rate over the lifespan of the volcano. We suspect that, over long timescales, steady subsidence and episodic uplift caused by magmatic intrusions counteract each other to produce the lower net subsidence rate indicated by the drill hole results.

5.3. Implications for Other Volcanoes and Future Work

[37] Our modeling shows that point sources of volume change (Mogi sources) and horizontal, rectangular uniform dilation sources (sills) fit the MLV leveling data equally well, presumably because the source is too deep (~10 km) for its geometry to be constrained by vertical surface displacements alone. A common characteristic of all best fit models is that sills require less subsurface volume change

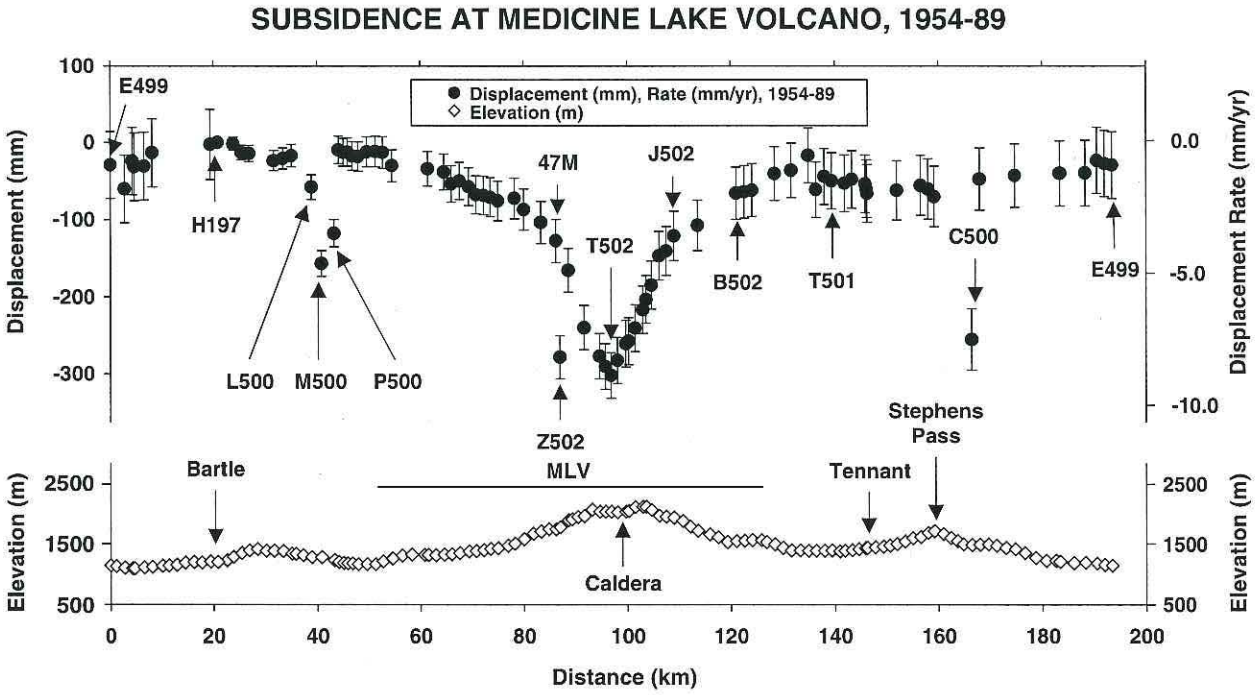

Figure 4. Vertical displacements and average displacement rates relative to datum point H197 near Bartle (left and right scales, respectively) obtained by comparing results of leveling surveys in 1954 and 1989 (top, circles), plus topography (bottom, diamonds), along a 193 km circuit across Medicine Lake volcano and Stephens Pass by way of Bartle, Hambone, Medicine Lake volcano, and Tennant (MLV circuit). Distance is measured counterclockwise along the leveling circuit starting at benchmark E499, which appears at both the left and right ends of the circuit. Error bars are one standard deviation from length-dependent random surveying error [*Vanicek et al.*, 1980] plus time-dependent benchmark instability [*Wyatt*, 1989], as discussed in the text. Benchmarks between B502 and T501 are common to the MLV circuit and the LBNM traverse (Figure 3). Anomalous movement of Z502 was probably caused by human disturbance, whereas the movements of C500, P500, M500, and L500 are attributed to faulting. Subsidence by a maximum of -302 ± 30 mm relative to H197, which corresponds to an average rate of -8.6 ± 0.9 mm/yr, is centered in the summit caldera (T502) and extends across the entire volcano. For consistency with *Dzurisin et al.* [1991], H197 was used as the datum point for calculating displacements and length-dependent errors; E499 was used for modeling. Displacements and displacement rates shown in Figures 7 and 8 are relative to E499, not H197 as here.

addition, we present results of the 1990 and 1999 leveling surveys, which reveal the 1954–1990 deformation pattern on the north flank of MLV and confirm ongoing, steady subsidence centered in the summit area during 1989–1999, respectively.

3.3. MLV Circuit, Corrected Results for 1954–1989

[15] During our analysis we discovered three spurious offsets in the 1954 data set used by *Dzurisin et al.* [1991] for comparison to the 1989 survey. The MLV circuit comprises NGS line number L15430, parts 3–6 (Figure 3). *Dzurisin et al.* [1991] failed to recognize that different reference elevations were used for each part of the line, which has the effect of introducing offsets in the elevation data where adjacent parts come together. We identified and removed these offsets by noting that, at each junction between parts, at least one benchmark was common to both parts. Setting the elevations of common marks equal in both parts and making the corresponding adjustments to other benchmark elevations allowed us to remove the following offsets from the 1954 data set (counterclockwise around the circuit starting near Bartle) (Figure 3): +0.08781 m from part 6 to part 5 (between Y500 and P503), +0.00438 m from part 5 to part 4 (between F502 and B502), and −0.08829 m from part 4 to part 3 (between T501 and N501). Note that the net offset around the circuit is only +0.0039 m (+3.9 mm). This partly explains why *Dzurisin et al.* [1991] failed to recognize the offsets: one was relatively small (+4.4 mm from part 5 to part 4), and the other two were nearly equal in magnitude but opposite in sign. As a result, the net offset around the entire circuit was negligible and differencing with the 1989 data produced a displacement profile that returned to near zero in the vicinity of datum point H197 near Bartle. Another factor that played a role is that the two large offsets occurred in places where recent faulting seemed plausible: 1) near the epicentral area of the 1981 Tennant swarm, and 2) near a group of young normal faults about 30 km south–southeast of the summit.

[16] A corrected elevation-change profile (Figure 4) was produced by subtracting the elevations relative to H197

determined by the 1954 survey from those determined by the 1989 survey and plotting the differences as a function of distance measured counterclockwise around the circuit from E499 (~15 km W of Bartle, Figure 1). H197 was used as the datum point for consistency with *Dzurisin et al.* [1991], while E499 was more convenient as a starting point for modeling. Figure 4 is similar to Figure 5 of *Dzurisin et al.* [1991], except that the spurious offsets described above do not appear in Figure 4 and distances along the leveling route are measured from different benchmarks (E499 and H197, respectively). Several features are apparent in Figure 4: 1) T502 subsided 302 ± 30 mm with respect to H197 at an average rate of −8.6 ± 0.9 mm/yr from 1954 to 1989; 2) subsidence extended across the entire volcano, not just its summit caldera; 3) localized displacements occurred at C500 ~ 7 km SSE of Stephens Pass; at Z502 ~ 10 km SSE of Medicine Lake; and at P500, M500, and L500 between Hambone and Julia Glover Flat, ~20 km ENE of Bartle; and 4) the displacement and elevation profiles are inversely related across the volcano but not across Stephens Pass.

[17] In most cases, anomalous movement of a single benchmark like that which occurred at C500 and Z502 can reasonably be attributed to benchmark instability and ignored. This is probably true for Z502, which is located in a concrete post in an open area at a road intersection and thus is susceptible to disturbance by logging equipment or other vehicles. C500 is also set in a concrete post, but it is less accessible and within the epicentral area of the 1978 Stephens Pass earthquake swarm, very close to the fissures that opened across Stephens Pass Road during the swarm. For this reason, we suspect that the anomalous movement of C500 was caused by the earthquakes rather than by cultural disturbance. Ground shaking might have induced the movement, but we modeled it with a fault dislocation that is consistent with the distribution of hypocenters and their focal mechanisms (see section 4). We also suspect that the anomalous movements of P500, M500, and L500 were caused by post-1954 movement along faults that form the west side of a large north-trending graben in the area. The southern 25 km of the Giant Crater lava field, which erupted from the south flank of MLV during a brief span of time about 10,500 ^{14}C yr B.P., was confined within the graben and is responsible for the present-day morphology of Julia Glover Flat [*Donnelly-Nolan et al.*, 1991]. No unusual seismicity has been recorded in the vicinity of the graben faults (Figure 2). On the other hand, Quaternary offsets of beds across the faults and their youthful morphologies are permissive of the idea that they have been active since 1954, probably sometime before the 1978 Stephens Pass earthquake swarm. We modeled the movements of P500, M500, and L500 with a dislocation near the west side of the graben, although the lack of recorded seismicity in the area leaves open the possibility that the movements were caused by benchmark instability rather than faulting.

[18] The inverse relationship between displacement and elevation along part of the leveling circuit suggests the possibility of systematic, slope dependent error in one or both of the surveys [*Stein*, 1981]. However, *Dzurisin et al.* [1991, Appendix] addressed this issue in detail and concluded that slope-dependent error accounts for no more than one third of the 1954–1989 subsidence. This result is not affected by the offset problem mentioned above. Nevertheless, resolution of this nagging issue was a primary motivation for the 1999 survey. Limited resources precluded measuring the entire circuit in 1999. Instead, we surveyed the 23-km-long summit traverse (Figure 3) because nearly half of the 1954–1989 subsidence occurred along this segment, which represents only 12% of the circuit. Different levels and rods were used for all three surveys (1954, 1989, and 1999), so the only common element that could cause uncorrected systematic error is slope-dependent refraction. Refraction corrections based on air temperature measurements at two heights above the ground at every setup were applied to the 1989 and 1999 data, so it is very unlikely that residual refraction error accounts for essentially the same result from 1954 to 1989 and 1989 to 1999 (see section 3.5).

3.4. LBNM Traverse, 1954–1990

[19] Because the MLV circuit does not cross the NE half of the volcano, it was unclear from the 1954–1989 results whether the subsidence pattern is radially symmetric or perhaps elongate N–S, parallel to regional faulting. The 1990 survey crossed the north flank of MLV and thus helps to resolve this issue. Maximum subsidence along the traverse (−139 ± 36 mm with respect to H197, or −3.9 ± 1.0 mm/yr) occurs at G504, ~10 km NNE of T502 (Figure 5). To convert the relative displacement measured between A13 at Weed and G504 to a displacement with respect to H197, we used the 1989 result for B502, which was included in all three surveys. Accordingly, the uncertainties listed above were calculated using the shortest distance along the leveling route from H197 to G504 by way of B502, even though the 1990 survey did not include H197. The 1954–1990 LBNM displacement profile is smooth, with no evidence for surface faulting during that period. Its shape is consistent with a radially symmetric pattern of subsidence centered within the caldera near T502 (see section 4).

3.5. MLV Summit Traverse, 1989–1999

[20] Based on the shapes of the MLV circuit and the 1954–1989 displacement profile (Figures 3 and 4), we elected to remeasure the dogleg-shaped segment of the MLV circuit between J502 and 47M, which crosses the southwest part of the summit caldera, in July 1999. Figure 6 shows the vertical displacements relative to 47M measured along this summit traverse from 1989 to 1999, and also the displacements predicted by linear extrapolation of the 1954–1989 results. To the extent that these results agree with one another, subsidence in the summit area from 1989 to 1999 was a steady continuation of the pattern observed from 1954 to 1989. In fact, the two displacement profiles are identical within two standard deviations at all of the benchmarks except Z502. Recall that Z502 moved anomalously during 1954–1989, which accounts for its unusual position along the predicted profile in Figure 6. The measured displacement of Z502 during 1989–1999 is consistent with the pattern of nearby benchmarks, which suggests that Z502 behaved normally during that period. We conclude that the average rate and pattern of subsidence in the summit area were the same during 1954–1989 and 1989–1999, and therefore that subsidence is a relatively steady process over decadal timescales. From August 1988

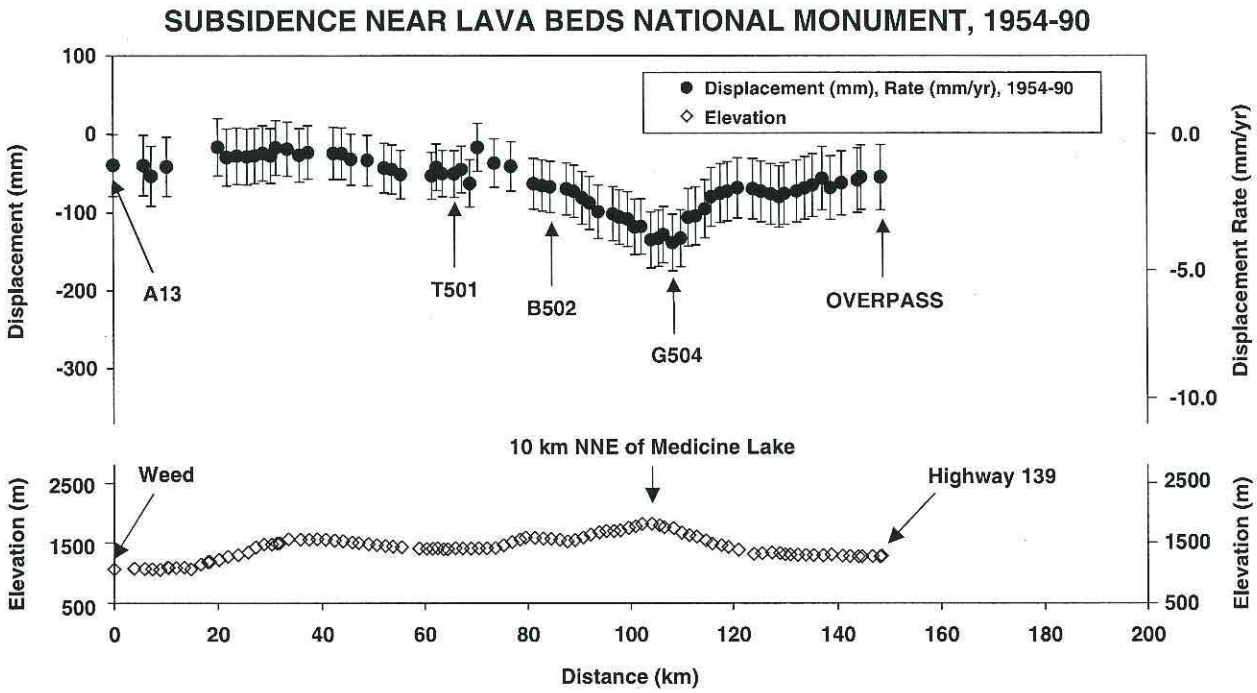

Figure 5. Vertical displacements and average displacement rates relative to datum point H197 near Bartle (left and right scales, respectively) from 1954 to 1990 (top, circles), plus topography (bottom, diamonds), along a 148 km east–west leveling traverse between Weed and California Highway 139 through Lava Beds National Monument (LBNM traverse). Error bars are one standard deviation from length-dependent random surveying error [*Vanicek et al.*, 1980] plus time-dependent benchmark instability [*Wyatt*, 1989], as discussed in the text. The segment between T501 and B502 is common to the MLV circuit and the LBNM traverse (Figure 3). Maximum subsidence relative to H197, -139 ± 36 mm (-3.9 ± 1.0 mm/yr) at G504, was calculated using the 1954–1989 displacement of B502 relative to H197 (Figure 4).

to October 1988 and from August 1988 to August 1989, including the 1988–1989 Medicine Lake swarm, the subsidence rate might have been about a factor of two higher (see section 3.2) [*Dzurisin et al.*, 1991].

4. Modeling Results

[21] *Dzurisin et al.* [1991] modeled the 1954–1989 leveling circuit by inverting the data to fit one or two point sources of volume change in an elastic half-space [*Mogi*, 1958]. They modeled two data sets separately: 1) all of the data, including those benchmarks affected by faulting or analysis errors, using one and then two point sources, and 2) data from only those benchmarks within 25 km of T502, none of which were affected by faulting or errors. In the second case, the best fit Mogi source was located 9 km beneath the caldera and represented a volume decrease of 0.140 km^3 (0.004 km^3/yr). Adding a second source did not significantly improve the fit. In hindsight, this is the only appropriate model because the others were affected by spurious offsets that made it appear that the entire volcano was downfaulted 5–10 cm relative to the surrounding plateau.

[22] For this study, we modeled the corrected 1954–1989 displacements using the inversion technique described by *Arnadottir et al.* [1992] and demonstrated in *Arnadottir and Segall* [1994] and *Bürgmann et al.* [1997]. The technique uses a constrained, nonlinear optimization algorithm that minimizes the weighted-residual sum of squares, $r^T \cdot \Sigma^{-1} \cdot r$, to determine the best fitting source location and additional parameters (volume change for a Mogi source; length, width, strike, dip and opening or slip for a dislocation source), where r is the residual vector between modeled and measured elevation changes at each benchmark, r^T represents the transpose of the residual vector, and Σ^{-1} represents the inverse of the data covariance matrix. The approach assumes that measured elevation changes contain correlated errors, which are accounted for by weighting the misfit using the inverse of the covariance matrix [*Arnadottir et al.*, 1992]. For deformation sources, we used a point source of volume change [*Mogi*, 1958] and rectangular dislocations with uniform slip and opening [*Okada*, 1985], both in a homogeneous, isotropic, elastic half-space. Dislocations were used to simulate the effects of faults (slip $\neq$ 0), dikes (opening $\neq$ 0), and sills (dip = 0, opening $\neq$ 0).

[23] To account for broad downwarping centered in the caldera and the two occurrences of known or suspected surface faulting (near Stephens Pass and the Giant Crater lava field), we first modeled the 1954–1989 displacements using a Mogi source and two model dip–slip faults. All of

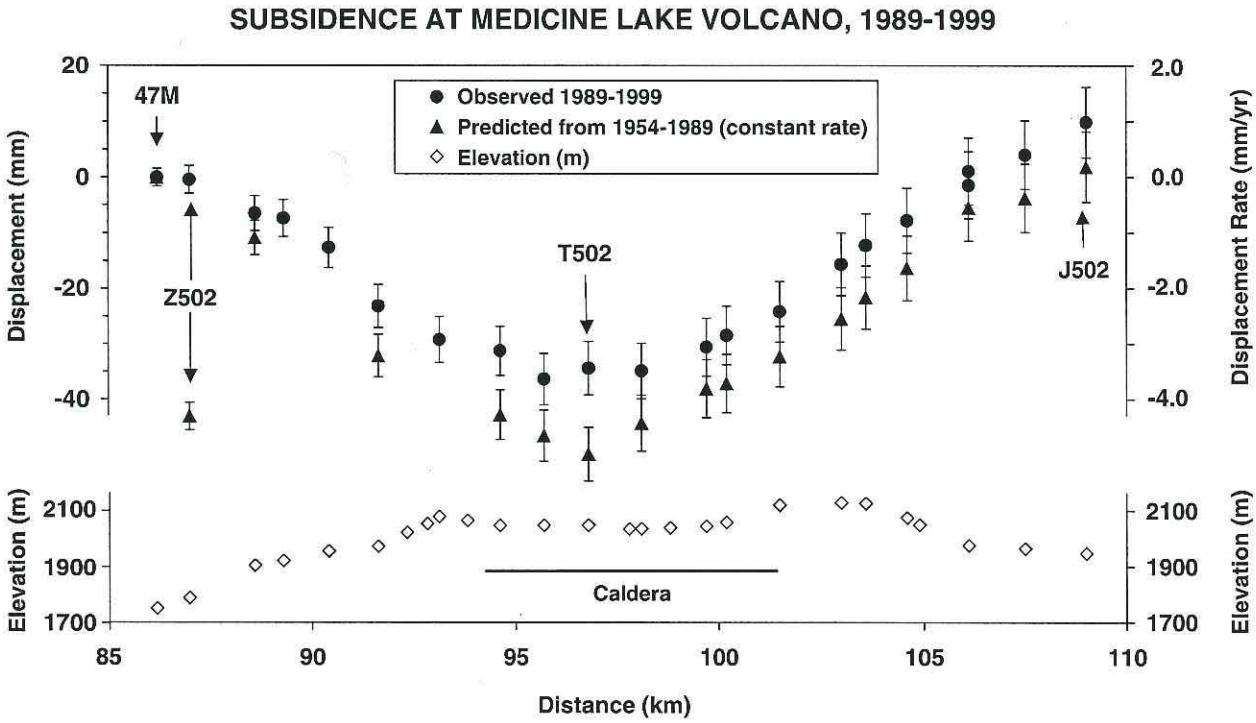

Figure 6. Measured and predicted vertical displacements and displacement rates relative to 47M for the period from 1989 to 1999 (top, circles and triangles, respectively), plus topography (bottom), along a 23 km leveling traverse across the summit area of Medicine Lake volcano. Distance is measured counterclockwise around the MLV circuit from H197 (same as Figure 4). Error bars (one standard deviation) include the effects of both length-dependent error [*Vanicek et al.*, 1980] and time-dependent error [*Wyatt*, 1989] as discussed in the text. Predicted displacements are based on the assumption that subsidence continued during 1989–1999 at the same rate as during 1954–1989. Except for Z502, which moved anomalously during 1954–1989 and is therefore discounted, all benchmarks were observed to subside at the predicted rate within two standard deviations in the measurements. Therefore, subsidence of MLV has been a relatively steady process over at least the past 5 decades and probably longer.

the benchmarks were included except Z502, which was apparently disturbed during that interval. Next, we inverted the 1954–1989 and 1989–1999 displacement-rate data separately using Mogi and sill sources. Finally, we inverted all of the data (1954–1989 MLV circuit, 1989–1999 MLV summit traverse, and 1954–1990 LBNM traverse) simultaneously using Mogi and sill sources. The results are useful for estimating source depths and volume changes, but do not realistically represent the mechanism(s) responsible for subsidence (see section 5).

4.1. 1954–1989 Displacements

[24] Three features are apparent in the 1954–1989 displacement data (Figures 4 and 7, top): 1) a symmetrical subsidence bowl centered at T502 near the summit of MLV, 2) an offset near C500 on the west flank of the volcano, and 3) offsets near L500, M500, and P500 near Julia Glover Flat (Figure 1), about 20 km ENE of Bartle. Displacement of C500 probably occurred during the 1978 Stephens Pass earthquake swarm, because the mark is located within the epicentral zone on the downthrown (east) side of surface cracks that formed during the swarm and all nearby marks are west of the cracks. On the other hand, no earthquakes have been recorded in the vicinity of L500, M500, or P500 (Figure 2). *Dzurisin et al.* [1991] suggested that the displacements measured there were caused by an unrecorded faulting episode sometime between 1954 and 1989, probably before the 1978 Stephens Pass swarm at a time when the seismic network was relatively sparse.

[25] To account for the observed subsidence and faulting, we inverted the 1954–1989 displacement data for one Mogi source and two dipping dislocations (Figure 7, top, solid line; Tables 1 and 2). The best fitting Mogi source is located 10 km beneath the southern part of the caldera floor and represents a volume decrease of 0.1129 ± 0.0046 km^3, which corresponds to a mean volumetric loss rate of 0.0032 ± 0.0001 km^3/yr. We modeled the displacement of C500 with an east-dipping dislocation that intersects the surface west of C500 but east of other nearby benchmarks (informally called the Stephens Pass fault). The model fault parameters (dip = 38°E, normal slip component = 0.90 ± 0.02 m) are generally consistent with both the distribution of 1981 hypocenters and the pattern of surface cracks, which suggest 1–1.5 m of dip–slip displacement on a N–S striking fault dipping 35–45°E [*Bennett et al.*, 1979]. Similarly, we modeled the displacements of L500,

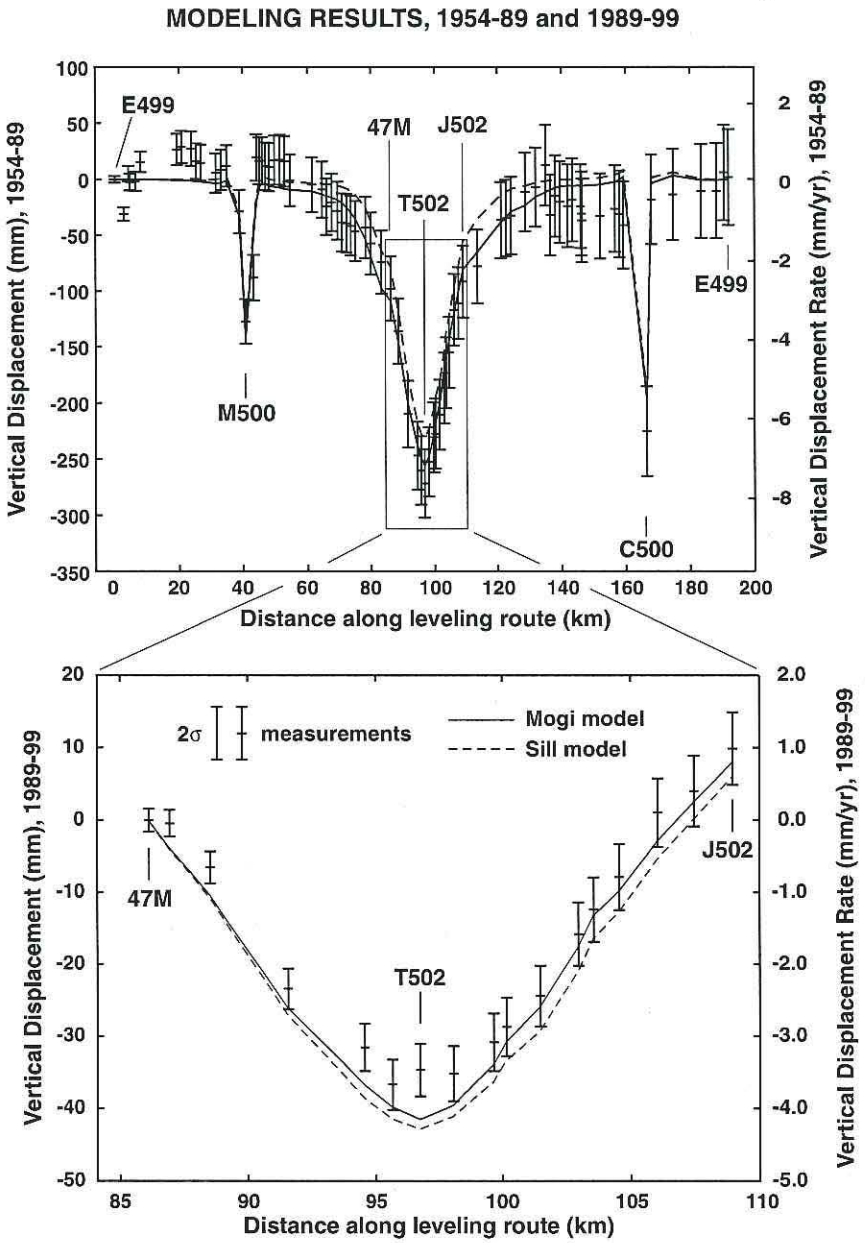

Figure 7. (Top) Vertical displacements and displacement rates (left and right scales, respectively) relative to E499 and best fit model curves for the Medicine Lake circuit, 1954–1989. Note that a different datum point (H197) was used for Figures 4 and 5. Deformation sources include a Mogi source at 10 km depth (solid curve) or a sill at 11 km depth (dashed curve) beneath the summit caldera, plus two normal faults near the periphery of the volcano. Source parameters are given in Tables 1 and 2. (Bottom) Vertical displacements and displacement rates relative to 47M compared to best fit Mogi (solid curve) and sill (dashed curve) sources for the Medicine Lake summit traverse, 1989–1999. Error bars (1-sigma) in both plots represent the combined effects of random surveying error, calculated using the distance measured counterclockwise around the circuit from E499 [*Vanicek et al.*, 1980], and benchmark vertical instability, which is assumed to be 0.5 mm/yr$^{1/2}$ · t (yr) [*Wyatt*, 1989]. Slight irregularities in the lines representing the model fits reflect changes in direction along the leveling route with respect to the source location. The inversion attempts to fit the slope of the elevation change between adjacent benchmarks, rather than the absolute displacement, so the model curves can be shifted up or down arbitrarily without affecting the model fit. We chose to reference the model curves here and in Figure 8 to specific benchmarks for convenience.

Table 1. Modeling Results for MLV Subsidence Source[a]

Data Set Modeled	Source Type	Latitude, °N	Longitude, °E	Depth, km	Length, km	Width, km	Dip, °	Strike, °	Opening, m/yr	Source-Volume Change, km^3	Source-Volume Change Rate, km^3/yr	WRSS	WRSS/(N − P)
1954–1989	Mogi	41.590	238.420	10.0	–	–	–	–	–	−0.1129 ± 0.0046	−0.0032 ± 0.0001	506.4	6.58
MLV Circuit	Sill	41.660–41.525	238.461–238.333	9.7	14.8	6.3	0	221	−0.0229 ± 0.0009	−0.0739 ± 0.0030	−0.0021 ± 0.0001	497.30	6.46
1989–1999	Mogi	41.590	238.420	10.0	–	–	–	–	–	−0.0280 ± 0.0017	−0.0028 ± 0.0002	10.03	0.63
Summit Traverse	Sill	41.666–41.523	238.464–238.339	7.7	14.9	7.7	0	189	−0.0112 ± 0.0010	−0.0128 ± 0.0011	−0.0013 ± 0.0001	9.43	0.59
1954–1999	Mogi	41.590	238.420	10.0	–	–	–	–	–	−0.1116 ± 0.0041	−0.0031 ± 0.0001	2836.92	18.31
All	Sill	41.566–41.637	238.441–238.590	11.0	10.3	4.4	0	221	−0.0446 ± 0.0014	−0.0903 ± 0.0028	−0.0020 ± 0.0001	2840.08	18.33

[a]WRSS = weighted residual sum of squares; $N - P$ = degrees of freedom. The sill model consistently yields smaller source-volume changes than the Mogi model, but for either model, the 1954–1989 and 1954–1999 volume change rates are identical within one standard deviation. The 1989–1999 rates derived from the much shorter summit traverse are somewhat lower than the 1954–1989 and 1954–1999 rates, but still within two standard deviations for the Mogi source. Apparently, subsidence has been relatively steady for several decades.

M500, and P500 as 0.41 ± 0.02 m of dip–slip movement on a normal fault dipping 45°E (unnamed fault in Figure 2; Table 2). The model fault is located near a mapped east-dipping fault that forms the west side of a N–S-trending graben between Hambone and Julia Glover Flat, about 20 km ENE of Bartle. The graben served as a channel for the Giant Crater lava field, which was emplaced during eruptions from the south flank of MLV about 10,500 ^{14}C yr B.P. [*Donnelly Nolan*, 1990, 1991].

[26] A model that includes a sill as the subsidence source (Figure 7, top, dotted line) fits the data only slightly better than the Mogi model (Tables 1 and 2). The best fit sill is located at nearly the same depth as the best fit Mogi source (9.7 km and 10.0 km, respectively), but requires one third less volume change to produce the same surface displacements (see section 5).

4.2. 1954–1989 and 1989–1999 Displacement Rates

[27] The 1999 survey did not include H197, which was used as the datum point for the 1954 and 1989 surveys, so the 1954–1989 and 1989–1999 data sets are not directly comparable. Nonetheless, we can model the shapes of the two displacement fields to invert for comparable source parameters. Our inversion of the 1989–1999 data using a Mogi source (Figure 7, bottom, solid line) produced the same source location and a similar average volume loss rate as our Mogi inversion of the 1954–1989 data (−0.0028 ± 0.0002 km^3/yr and −0.0032 ± 0.0001 km^3/yr, respectively; Table 1). On the other hand, sill models yield significantly different volume loss rates for the two time periods (−0.0013 ± 0.0001 km^3/yr for 1989–1999, −0.0021 ± 0.0001 km^3/yr for 1954–1989; Figure 7, bottom, dotted line). The sill derived from the 1989–1999 data is larger and shallower than that from the 1954–1989 data (Figure 2; Table 1). However, the 1989–1999 sill model is based on fewer data points (17 benchmarks) and is therefore less well constrained than the 1954–1989 sill model.

[28] We conclude that the subsidence source was stable from 1954 to 1999; so all three data sets (1954–1989 MLV circuit, 1954–1990 LBNM traverse, and 1989–1999 MLV summit traverse) can be combined to constrain a single model. However, the combined data set is temporally sparse and therefore the subsidence rate as a function of time is poorly constrained.

4.3. Combined Data Sets: 1954–1989, 1989–1999, and 1954–1990

[29] The inversion technique fits the slope of the elevation change between adjacent benchmarks (i.e., tilt) rather than the displacement of each mark relative to a datum point, so multiple data sets with different datum points can be combined in a single model. For modeling purposes, we split the 1954–1990 LBNM traverse into two data sets with different datum points, because part of the traverse (between T501 in the west to B502 in the east) was not measured in 1990. Thus, the global inversion included four data sets: 1) 1954–1989 MLV circuit, 2) 1989–1999 MLV summit traverse, 3) 1954–1990 LBNM traverse (west side), and 4) 1954–1990 LBNM traverse (east side). This approach gives appropriately greater weight to 17 summit-area benchmarks that were surveyed three times (1954,

Table 2. Modeling Results for Stephens Pass and Unnamed Fault Sources

Fault	Latitude at Center, °N	Longitude at Center, °E	Depth at Center, km	Length Along Strike, km	Width, km	Dip, °	Strike, °	Slip, m
Stephens Pass	41.50–41.42	238.16	2	8.9	2.5	38E	0	−0.90 ± 0.02
Unnamed	41.34–41.28	238.27	3	6.7	4.2	45E	0	−0.41 ± 0.02

1989, 1999) relative to others that were measured only twice.

[30] As with the individual data sets, we inverted the combined data set for both Mogi and sill sources. The best fit Mogi source is located under the south part of the caldera at a depth of 10 km. It has a slightly lower than the best fit sill, which is also located under the south caldera at a depth of 11 km (Figure 8; Table 1). The volume loss rates of the

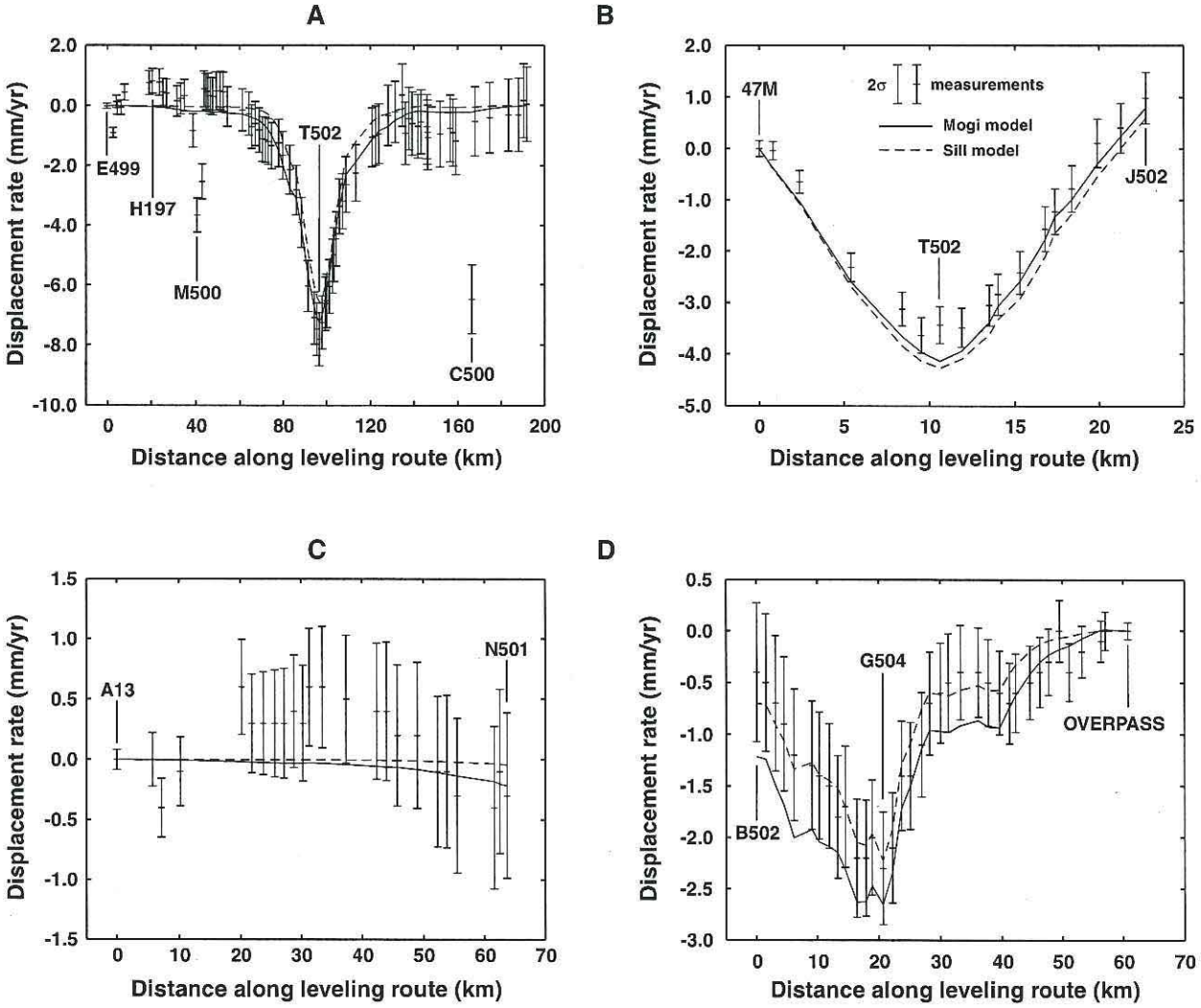

Figure 8. Displacement rate data and best fit model profiles for: A) the 1954–1989 MLV circuit relative to E499, B) the 1989–1999 MLV summit traverse relative to 47M, C) the western part of the 1954–1990 LVNM traverse relative to A13, and D) the eastern part of the 1954–1990 LVNM traverse relative to OVERPASS. Solid and dashed lines represent best fit Mogi and sill sources, respectively. Error bars (1 sigma) include the combined effects of random surveying error, calculated using the distance measured counterclockwise around the circuit from E499 [*Vanicek et al.*, 1980], and benchmark instability, which is assumed to be 0.5 mm/yr$^{1/2}$ · t (yr) [*Wyatt*, 1989]. Irregularities in the lines representing the model fits, which are especially evident in D, are caused by changes in direction along the leveling route with respect to the source location. The inversion fits the slope between adjacent data points rather than the data values (i.e., tilt rather than displacement), so the model curves can be shifted up or down arbitrarily. We chose to reference the model curves here and in Figure 7 to specific benchmarks for convenience.

two best fit sources are 0.0031 ± 0.0001 km^3/yr and 0.0020 ± 0.0001 km^3/yr, respectively. Consistent with our experience modeling the 1954–1989 data set separately, we found that including two or more Mogi or sill sources in the global inversion did not significantly improve the model fit to the data.

5. Discussion

5.1. Subsidence Mechanisms

[31] Possible mechanisms for volcano-wide subsidence at MLV include: 1) magma withdrawal, 2) contraction of hot crystalline rock during cooling, 3) densification of a cooling magma body during crystallization, 4) gravitational loading of the lithosphere by the MLV edifice and associated dense intrusive rocks, and 5) crustal thinning as a result of Basin and Range extension. *Dzurisin et al.* [1991] suggested that mafic magma might accumulate temporarily beneath MLV, cool, densify, then sink while still fluid to cause subsidence. Although this mechanism cannot be discounted entirely, there is no independent evidence for steady withdrawal of magma since 1954 and, as shown below, two other mechanisms that almost surely operate at MLV can account for the observed subsidence.

[32] The second mechanism, thermal contraction of a cooling mass of crystalline rock beneath MLV, cannot fully account for the observed subsidence. The coefficients of thermal expansion, α, for gabbro and granite under standard conditions are 1.6×10^{-5}/°C and 2.4×10^{-5}/°C, respectively [*Turcotte and Schubert*, 1982, p. 432]. The volume change, ΔV, in a volume of rock, V, cooling through a temperature range, ΔT, is given by: $\Delta V = \alpha \cdot V \cdot \Delta T$. Using $\Delta V = -0.0031$ km^3, the annual volume decrease beneath MLV from the Mogi model results above, and $\alpha = 1.6 \times 10^{-5}$/°C for gabbro (the most likely rock type at 10 km depth beneath MLV), we obtain: $V \cdot \Delta T = 187.5$ km^3°C. What is a plausible value for ΔT, the annual temperature decrease of a cooling pluton at 10 km depth? *Hayba and Ingebritsen* [1997] modeled multiphase groundwater flow near cooling plutons in two dimensions and showed that a 2 km × 4 km pluton emplaced at 5 km depth with an initial temperature of 900°C cooled to temperatures between ~250°C (edge) and ~850°C (center) in 25,000 years and between ~150°C and 550°C in 50,000 years. A maximum value for ΔT, the average annual temperature change of a pluton at 10 km depth (where cooling would be slower than at 5 km depth), is therefore [(250°C–900°C)/2.5×10^4 yr], or $\Delta T = -0.026$°C/yr. Using this value in the equation above, we obtain $V \approx 7200$ km^3, an implausibly large volume for a cooling pluton beneath MLV. We explored the possibility that α might be significantly larger at higher temperatures by using the program CONFLOW [*Mastin and Ghiorso*, 2000] to calculate density changes of the principal minerals comprising gabbro at near-magmatic temperatures. None of the calculated values for α exceed the value for gabbro used above by more than a factor of two. Therefore we conclude that the contribution of thermal contraction to subsidence at MLV is negligible.

[33] Crystallizing magma undergoes volume changes as crystals replace melt and volatiles partition into the declining melt fraction until saturation is reached. At that point bubbles form and either remain trapped in the melt or escape upward. The greatest volume decrease (~10%) occurs in the latter case [*Sigmundsson et al.*, 1997; *Sturkell and Sigmundsson*, 2000]. We used CONFLOW [*Mastin and Ghiorso*, 2000] to explore the implications of magma crystallization for subsidence at MLV. As input to the program, we used the major-oxide composition of Modoc Plateau high-alumina basalt [*Gerlach and Grove*, 1982], which *Donnelly-Nolan* [1988] believes is representative of the parental magma at MLV, and the H_2O content of the MLV Black Crater basalt reported by *Sisson and Layne* [1993] (0.2–0.3 wt.%). Our calculations show that MLV high-alumina basalt would contract by ~0.1% as the degree of crystallization increased from 50% to 51%, for example. To produce the observed annual volume change of −0.003 km^3/yr, a 3 km^3 magma body at 10 km would have to crystallize at a rate of ~1% per year, which is implausibly rapid according to the modeling results of *Hayba and Ingebritsen* [1997]. If such rapid crystallization were occurring at MLV, the subsidence rate would slow over decadal timescales as the residual melt became depleted. Such is the case at Askja and Krafla, Iceland, where posteruption subsidence rates are observed to be decreasing with time [*Sigmundsson et al.*, 1997; *Sturkell and Sigmundsson*, 2000]. The leveling results at MLV, on the contrary, show that the average subsidence rate during 1989–1999 was essentially the same as during 1954–1989. Furthermore, because the starting composition of MLV high-alumina basalt is relatively dry, the residual melt does not become volatile-saturated until crystallization is 94%–95% complete. Not until then do bubbles form and potentially reduce the volume of the residual melt through escape. We conclude that crystallization is not an important subsidence mechanism at MLV.

[34] *Dzurisin et al.* [1991] proposed two subsidence mechanisms at MLV: 1) gravitational loading of thermally weakened crust by the mass of the volcano and associated intrusive rocks, and 2) thinning of locally weakened crust due to Basin and Range extension. The MLV edifice is too young (500–600 ka) [*Donnelly Nolan*, 1998] to be gravitationally compensated, so loading almost surely contributes to contemporary subsidence. The resulting flexure should be analogous to that observed around the Hawaiian archipelago and other ocean islands, including subsidence centered at the edifice and a surrounding annulus of uplift [*Walcott*, 1970]. At MLV, the uplift annulus might be located outside the area covered by leveling or too small to detect. Likewise, Basin and Range extension is known to be occurring at MLV, so subsidence of subvolcanic crust that has been thermally weakened by repeated magmatic intrusions is to be expected. *Dzurisin et al.* [1991] envisioned a situation akin to a "hole in a plate" in which the hole represents a cylindrical zone of hot and mechanically weak crust beneath the volcano. As the plate extends, the weak zone thins and subsides under gravity. A quantitative analysis of loading and extension as subsidence mechanisms at MLV is underway.

5.2. Implications of Steady Subsidence for Longer-Term Behavior

[35] Leveling results suggest that the subsidence rate at MLV has been essentially constant for nearly five decades (based on measurements in 1954, 1988, 1989, 1990, and

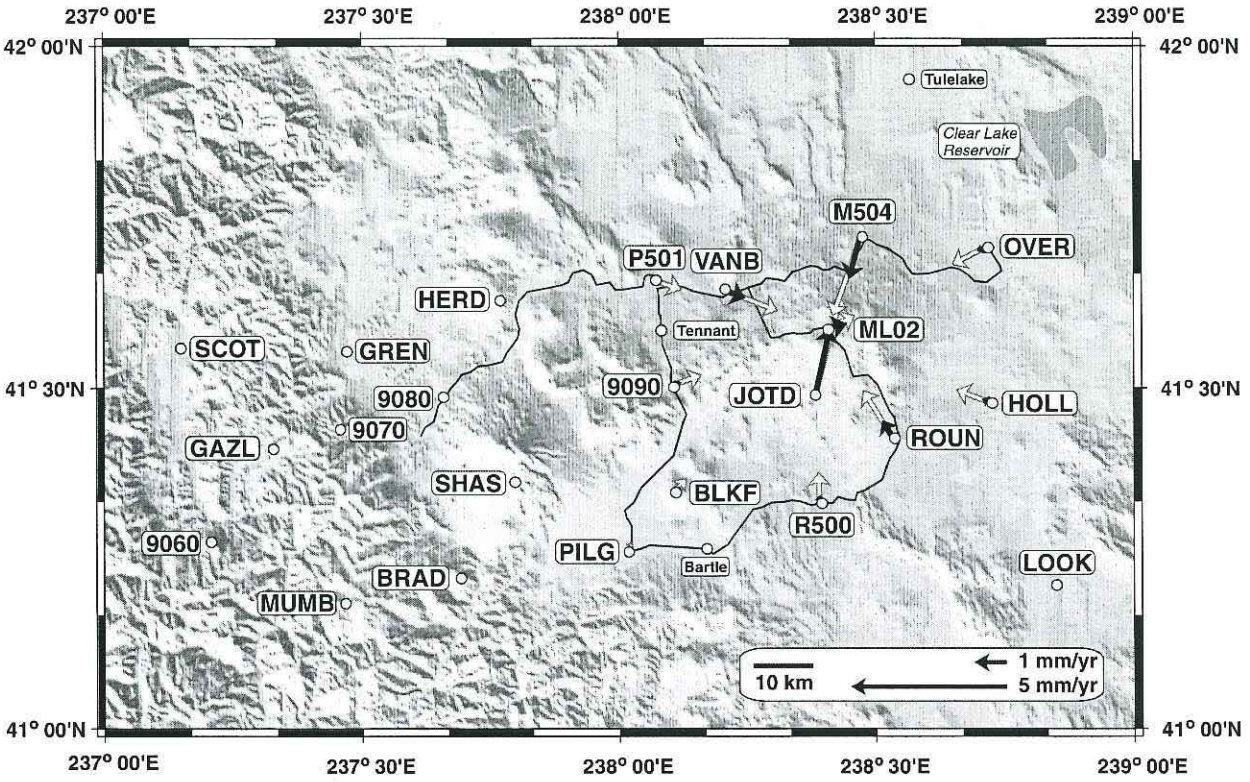

Figure 9. Predicted horizontal displacement rates at existing GPS stations based on the best fitting Mogi source (red arrows) and sill (black arrows).

1999 only), which raises the question of how far into the past the current rate should be extrapolated. For example, a constant subsidence rate of 8.6 ± 0.8 mm/yr would produce 8.6 ± 0.8 m of subsidence in 1,000 years and 860 ± 80 m of subsidence in 100,000 years. *Dzurisin et al.* [1991] reviewed the evidence for long-term subsidence of MLV from 8 drill holes, 5 of which penetrated the entire volcanic pile. They concluded that the crust beneath MLV has been downwarped ~500 m relative to the surrounding plateau. The current rate would have produced 500 m of subsidence in only ~60,000 years, approximately 10% of the lifespan of the volcano. It is highly unlikely that all of the subsidence would occur in the last 10% of the volcano's history, especially given that there is no obvious increase in eruptive productivity. Thus, the current rate of subsidence must be anomalous and either the subsidence rate has increased through time, the subsidence process has been episodic, or subsidence has been counterbalanced by uplift associated with intrusions.

[36] The relatively high rate of contemporary subsidence could be a recent phenomenon, i.e., a delayed response of the lithosphere to the increasing load imposed by the growing MLV edifice plus intrusive complex. For example, changes in the subsurface temperature distribution caused by intrusions or eruptions could lead to time-varying viscous strength of the crust. Extension could be responsible for a relatively minor amount of subsidence throughout the entire 500–600 ka lifespan of MLV, while gravitational loading by the mature volcanic system has only recently become the dominant mechanism and is largely responsible for the high contemporary subsidence rate. Alternatively, crustal extension might be the dominant cause of subsidence and the extension rate might have increased recently. In this scenario, gravitational loading produced a relatively minor, steady amount of subsidence as the volcano grew, while the crustal extension rate increased to produce the relatively high contemporary subsidence rate. Thus, the current anomalous subsidence rate could be explained by an unusually high crustal extension rate in the MLV region during Holocene time. This possibility is neither supported nor refuted by available data. Regardless of the subsidence mechanism, the historical rate of subsidence is clearly greater than the average rate over the lifespan of the volcano. We suspect that, over long timescales, steady subsidence and episodic uplift caused by magmatic intrusions counteract each other to produce the lower net subsidence rate indicated by the drill hole results.

5.3. Implications for Other Volcanoes and Future Work

[37] Our modeling shows that point sources of volume change (Mogi sources) and horizontal, rectangular uniform dilation sources (sills) fit the MLV leveling data equally well, presumably because the source is too deep (~10 km) for its geometry to be constrained by vertical surface displacements alone. A common characteristic of all best fit models is that sills require less subsurface volume change

than Mogi sources to produce the same amount of vertical surface displacement, a relationship that was previously noted by *Delaney and McTigue* [1994] in their analysis of deformation at Kilauea volcano in Hawaii. *Dieterich and Decker* [1975] used finite element modeling to analyze the surface effects of various sources, including sills and Mogi sources, and concluded that vertical displacement data alone are not sufficient to constrain the depth, volume/pressure change, and geometry of the deformation source(s). With this in mind, the USGS Cascades Volcano Observatory established a network of GPS stations in the MLV–Mount Shasta region in July 1990 to measure three-dimensional surface displacements. The network has since been expanded and remeasured twice [*Poland et al.*, 2000; *Poland*, 2001].

[38] We used the best fitting Mogi and sill sources from this study to predict horizontal displacement rates at benchmarks included in the MLV–Mount Shasta network. The sources produce similar vertical displacement rates, but significantly different horizontal rates at some locations (Figure 9). Both produce horizontal velocity vectors that generally point toward the summit, reach a maximum near the caldera rim, and decrease both inward and outward from there. However, at some sites the Mogi source predicts horizontal velocities that are several times larger than those predicted by the sill source. This is because the magnitudes of vertical and horizontal forces produced by a Mogi source are equal, whereas horizontal forces produced by a sill are much smaller than the corresponding vertical forces. As a result, the surface volume change exceeds the source volume change for a Mogi source, but for a sill these two volumes are essentially equal (i.e., a Mogi source produces host-rock dilatation but a sill source does not) [*Delaney and McTigue*, 1994]. As a consequence of this difference, repeated GPS surveys at MLV will help to distinguish between a Mogi and sill source. Preliminary results of simultaneous inversion of GPS and leveling data favor a Mogi source of deflation at 10 km depth [*Poland*, 2001], which is consistent with the modeling results presented above.

[39] Each of the subsidence mechanisms discussed above is expected to operate to varying degrees at other Cascade volcanoes, particularly Newberry in central Oregon, which is similar in many respects to MLV. Both volcanoes are located ~50 km east of the Cascade axis near the western margin of the Basin and Range, are broad shields marked with summit calderas, contain abundant rhyolitic domes and flows in addition to more areally extensive basalt and basaltic-andesite flows, have similar petrochemistry, and have been the sites of eruptions of pumiceous tephra and obsidian flows during the last few thousand years [*Macleod et al.*, 1981]. The effects of gravitational loading and crustal extension, in particular, should be analogous at the two volcanoes. However, comparison of leveling surveys across Newberry volcano suggests as much as 97 ± 22 mm of uplift between 1931 and 1994, contrary to the results at MLV [*Dzurisin*, 1999]. Another leveling survey across Newberry volcano is planned to confirm this apparent difference and explore its causes. Although gravitational loading, regional deformation, cooling of intrusive rock, and magma crystallization are not directly linked to eruptive processes, they are important parts of the eruption cycle that deserve more study in the Cascade Range and elsewhere.

[40] **Acknowledgments.** The authors wish to thank the 1999 Medicine Lake leveling crew for their hard work and good cheer: Stuart Ashbaugh, Miya Barr, Adam Cook, Chris Harpel, Sean Taylor, Dave Wieprecht, and Ken Yamashita. Julie Donnelly-Nolan shared her insights into the geologic history of MLV, which were invaluable in guiding our thinking about the implications of our results. We are grateful to USGS technical reviewers Marianne Guffanti and Larry Mastin for their constructive comments on an early draft of the manuscript, and to Mastin for guidance in our use of program CONFLOW. Two anonymous reviewers and Associate Editor Jeff Freymueller encouraged us to improve section 5 by considering alternative subsidence mechanisms. We appreciate their diligence and constructive comments. Figures 1, 2, and 9 were created using Generic Mapping Tools (GMT) [*Wessel and Smith*, 1998]. This research was supported in part by the USGS Volcano Hazards Program. Poland was supported in part by a National Defense Science and Engineering Graduate Fellowship.

References

Argus, D. F., and R. Gordon, Pacific–North American Plate motion from very long baseline interferometry compared with motion inferred from magnetic anomalies, transform faults and earthquake slip vectors, *J. Geophys. Res.*, *95*, 17,315–17,324, 1991.

Arnadottir, T., and P. Segall, The 1989 Loma Prieta earthquake imaged from inversion of geodetic data, *J. Geophys. Res.*, *99*, 21,835–21,855, 1994.

Arnadottir, T., P. Segall, and M. Matthews, Resolving the discrepancy between geodetic and seismic fault models for the 1989 Loma Prieta, California, earthquake, *Bull. Seismol. Soc. Am.*, *82*, 2248–2255, 1992.

Balazs, E. I., and G. M. Young, Corrections applied by the National Geodetic Survey to precise leveling observations, *Tech. Memo. NOS NGS 34*, 12 pp., Natl. Oceanic and Atmos. Admin., Boulder, Colo., 1982.

Bennett, J. H., R. W. Sherburne, C. H. Cramer, C. W. Chesterman, and R. H. Chapman, Stephens Pass earthquakes, Mount Shasta—August 1978, *Calif. Geol.*, *32*, 27–34, 1979.

Bennett, R. A., B. P. Wernicke, and J. L. Davis, Continuous GPS measurements of contemporary deformation across the northern Basin and Range province, *Geophys. Res. Lett.*, *25*, 563–566, 1998.

Blakely, R. J., R. L. Christiansen, M. Guffanti, R. E. Wells, J. M. Donnelly-Nolan, L. J. P. Muffler, M. A. Clynne, and J. G. Smith, Gravity anomalies, Quaternary vents, Quaternary faults in the southern Cascade Range, Oregon and California: Implications for arc and backarc evolution, *J. Geophys. Res.*, *102*, 22,513–22,527, 1997.

Bolt, B. A., and R. D. Miller, Catalogue of earthquakes in northern California and adjoining areas, 1 January 1910–31 December 1972, Seismographic stations, Rep., Univ. of Calif. Berkeley, Berkeley, 1975.

Bürgmann, R., P. Segall, M. Lisowski, and J. Svarc, Postseismic strain following the 1989 Loma Prieta earthquake from GPS and leveling measurements, *J. Geophys. Res.*, *102*, 4933–4955, 1997.

Cramer, C. H., Stephens Pass earthquake swarm of August 1978, east of Mount Shasta, California, (abstract), *Eos Trans. AGU*, *59*, 1130, 1978.

Delaney, P. T., and D. F. McTigue, Volume of magma accumulation or withdrawal estimated from surface uplift or subsidence, with application to the 1960 collapse of Kilauea Volcano, *Bull. Volcanol.*, *56*, 417–424, 1994.

Dieterich, J. H., and R. W. Decker, Finite element modeling of surface deformation associated with volcanism, *J. Geophys. Res.*, *80*, 4094–4102, 1975.

Dixon, T. H., S. Robaudo, J. Lee, and M. C. Reheis, Constraints on present-day Basin and Range deformation from space geodesy, *Tectonics*, *14*, 755–772, 1995.

Dixon, T. H., M. M. Miller, F. Farina, H. Wang, and D. J. Johnson, Present-day motion of the Sierra Nevada block and some tectonic implications for the Basin and Range province, North American Cordillera, *Tectonics*, *19*, 1–24, 2000.

Donnelly-Nolan, J. M., A magmatic model of Medicine Lake volcano, California, *J. Geophys. Res.*, *93*, 4412–4420, 1988.

Donnelly-Nolan, J. M., Abrupt shifts in $\delta^{18}O$ values at Medicine Lake volcano (California, USA), *Bull. Volcanol.*, *59*, 529–536, 1998.

Donnelly-Nolan, J. M., D. E. Champion, C. D. Miller, T. L. Grove, and D. A. Trimble, Post-11,000-year volcanism at Medicine Lake volcano, Cascade Range, Northern California, *J. Geophys. Res.*, *95*, 19,693–19,704, 1990.

Donnelly-Nolan, J. M., D. E. Champion, C. D. Miller, T. L. Grove, M. B. Baker, J. E. Taggart Jr., and P. E. Bruggman, The Giant Crater lava field: Geology and geochemistry of a compositionally-zoned, high-alumina

basalt to basaltic andesite eruption at Medicine Lake volcano, California, *J. Geophys. Res.*, *96*, 21,843–21,863, 1991.

Dzurisin, D., Results of repeated leveling surveys at Newberry volcano, Oregon, near Lassen Peak volcano, California, *Bull. Volcanol.*, *61*, 83–91, 1999.

Dzurisin, D., J. M. Donnelly-Nolan, J. R. Evans, S. R. Walter, and D. Dzurisin, Crustal subsidence, seismicity, structure near Medicine Lake volcano, California, *J. Geophys. Res.*, *96*, 16,319–16,333, 1991.

Evans, J. R., and J. J. Zucca, Active high-resolution seismic tomography of compressional wave velocity and attenuation structure at Medicine Lake volcano, northern California Cascade Range, *J. Geophys. Res.*, *93*, 15,016–15,036, 1998.

Federal Geodetic Control Committee, J. D. Bossler, (chairman), Standards and specifications for geodetic control networks, Rep., Natl. Oceanic and Atmos. Admin., Rockville, Md., 1984.

Finn, C., and D. L. Williams, Gravity evidence for a shallow intrusion under Medicine Lake volcano, California, *Geology*, *10*, 503–507, 1982.

Gerlach, D. C., and T. L. Grove, Petrology of Medicine Lake Highland volcanics: Characterization of endmembers of magma mixing, *Contrib. Mineral. Petrol.*, *80*, 147–159, 1982.

Hayba, D. O., and S. E. Ingebritsen, Multiphase groundwater flow near cooling plutons, *J. Geophys. Res.*, *102*, 12,235–12,252, 1997.

MacLeod, N. S., D. R. Sherrod, L. A. Chitwood, and E. H. McKee, Newberry Volcano, Oregon, in *Guides to Some Volcanic Terranes in Washington, Idaho, Oregon, Northern California, U.S. Geol. Surv. Circ.*, C838, 85–91, 1981.

Mastin, L. G., and M. S. Ghiorso, A numerical program for steady-state flow of magma-gas mixtures through vertical eruptive conduits, *U.S. Geol. Surv. Open File Rep., 00-209*, 61 pp., 2000.

Miller, M. M., D. J. Johnson, C. M. Rubin, H. Dragert, K. Wang, A. Qamar, and C. Goldfinger, GPS-determination of along-strike variation in Cascadia margin kinematics: Implications for relative plate motion, subduction zone coupling, permanent deformation, *Tectonics*, *20*, 161–176, 2001.

Minster, J. B., and T. H. Jordon, Vector constraints on western U.S. deformation from space geodesy, neotectonics, plate motions, *J. Geophys. Res.*, *92*, 4798–4804, 1987.

Mogi, K., Relations between the eruptions of various volcanoes and the deformations of the ground surface around them, *Bull. Earthquake Res. Inst. Univ. Tokyo*, *36*, 99–134, 1958.

Okada, Y., Surface deformation due to shear and tensile faults in a half-space, *Bull. Seismol. Soc. Am.*, *75*(4), 1135–1154, 1985.

Poland, M. P., Determining the stress regime within a volcanic edifice from igneous intrusions and deformation measurements, Ph.D. thesis, Ariz. State Univ., Tempe, Ariz., 2001.

Poland, M. P., D. Dzurisin, R. Bürgmann, E. Koenig, and J. H. Fink, Modeling deformation at Medicine Lake volcano in northern California using regional tectonic and local volcanic sources, *Eos Trans. AGU*, *81*(48), F338, Fall Meet. Suppl., Abstract, 2000.

Ritter, J. R. R., and J. R. Evans, Deep structure of Medicine Lake volcano, California, *Tectonophysics*, *275*, 221–241, 1997.

Schomaker, M. C., and R. M. Berry, *Geodetic Leveling, Manual NOS NGS 3*, Natl. Geod. Surv., Natl. Oceanic and Atmos. Admin., Rockville, Md., 1981.

Sigmundsson, F., H. Vadon, and D. Massonnet, Readjustment of the Krafla spreading segment to crustal rifting measured by satellite radar interferometry, *Geophys. Res. Lett.*, *24*, 1843–1846, 1997.

Sisson, T. W., and G. D. Layne, H_2O in basalt and basaltic andesite glass inclusions from four subduction-related volcanoes, *Earth Planet. Sci. Lett.*, *117*, 619–635, 1993.

Stein, R. S., Discrimination of tectonic displacement from slope-dependent errors in geodetic leveling from southern California, 1953–1977, in *Earthquake Prediction: An International Review, Maurice Ewing Ser.*, vol. 4, edited by D. W. Simpson and P. G. Richards, pp. 441–456, AGU, Washington, D. C., 1981.

Strange, W. E., The effect of systematic errors on geodynamic analysis, in *Second International Symposium on Problems Related to the Redefinition of North American Vertical Geodetic Networks*, pp. 704–729, Can. Inst. of Surv., Surv. and Mapp. Branch, Ottawa, 1980a.

Strange, W. E., The impact of refraction corrections on leveling interpretations in California(abstract), *Eos Trans. AGU*, *61*, 365, 1980b.

Sturkell, E., and F. Sigmundsson, Continuous deflation of the Askja Caldera, Iceland, during the 1983–1998 noneruptive period, *J. Geophys. Res.*, *105*, 25,671–25,684, 2000.

Thatcher, W., G. R. Foulger, B. R. Julian, J. Svarc, E. Quilty, and G. W. Bawden, Present-day deformation across the Basin and Range province, western United States, *Science*, *283*, 1714–1718, 1999.

Turcotte, D. L., and G. Schubert, *Geodynamics, Applications of Continuum Physics to Geological Problems*, 450 pp., John Wiley, New York, 1982.

Vanicek, P., R. O. Castle, and E. I. Balazs, Geodetic leveling and its applications, *Rev. Geophys.*, *18*, 505–524, 1980.

Walcott, R. I., Flexure of lithosphere at Hawaii, *Tectonophysics 9*, 435–446, 1970.

Walter, S., and D. Dzurisin, The September 1988 earthquake swarm at Medicine Lake volcano, northern California(abstract), *Eos Trans. AGU*, *70*, 1189–1190, 1989.

Wessel, P., and W. H. F. Smith, New, improved version of Generic Mapping Tools released, *Eos Trans. AGU*, *79*, 579, 1998.

Wyatt, F. W., Displacement of surface monuments: Vertical motion, *J. Geophys. Res.*, *94*, 1655–1664, 1989.

Zoback, M. L., First- and second-order patterns of stress in the lithosphere: The World Stress Map Project, *J. Geophys. Res.*, *97*, 11,703–11,728, 1992.

Zoback, M. L., and M. D. Zoback, Tectonic stress field of the continental United States, in *Geophysical Framework of the Continental United States, Geol. Soc. Am. Mem.*, vol. 172, edited L. C. Pakiser and W. D. Mooney, pp. 523–540, Geol. Soc. of Am., Boulder, Colo., 1989.

R. Bürgmann, Department of Earth and Planetary Science, University of California, Berkeley, 385 McCone Hall, Berkeley, CA 94720-4767, USA. (burgmann@seismo.berkeley.edu)

D. Dzurisin and M. P. Poland, U.S. Geological Survey, David A. Johnston Cascades Volcano Observatory (USGS/CVO), 1300 SE Cardinal Court, Building 10, Suite 100, Vancouver, WA 98683-9589, USA. (dzurisin@usgs.gov; mpoland@usgs.gov)